AGU PUBLICATIONS

Geophysical Research Letters

RESEARCH LETTER
10.1002/2017GL075399

Key Points:
- High daily runoff in the western United States occurs primarily in response to atmospheric rivers
- The probability of high runoff and maximum daily runoff increases with water vapor transport
- Runoff response to atmospheric rivers has systematic seasonal and geographic variation

Supporting Information:
- Supporting Information S1

Correspondence to:
C. P. Konrad,
cpkonrad@usgs.gov

Citation:
Konrad, C. P., & Dettinger, M. D. (2017). Flood runoff in relation to water vapor transport by atmospheric rivers over the western United States, 1949–2015. *Geophysical Research Letters, 44*, 11,456–11,462. https://doi.org/10.1002/2017GL075399

Received 21 AUG 2017
Accepted 10 NOV 2017
Accepted article online 15 NOV 2017
Published online 29 NOV 2017

Flood Runoff in Relation to Water Vapor Transport by Atmospheric Rivers Over the Western United States, 1949–2015

Christopher P. Konrad[1] **and Michael D. Dettinger**[2,3]

[1]U.S. Geological Survey, Tacoma, WA, USA, [2]U.S. Geological Survey, Carson, NV, USA, [3]Scripps Institution of Oceanography, University of California, San Diego, La Jolla, CA, USA

Abstract Atmospheric rivers (ARs) have a significant role in generating floods across the western United States. We analyze daily streamflow for water years 1949 to 2015 from 5,477 gages in relation to water vapor transport by ARs using a 6 h chronology resolved to 2.5° latitude and longitude. The probability that an AR will generate 50 mm/d of runoff in a river on the Pacific Coast increases from 12% when daily mean water vapor transport, *DVT*, is greater than 300 kg m^{-1} s^{-1} to 54% when DVT > 600 kg m^{-1} s^{-1}. Extreme runoff, represented by the 99th quantile of daily values, doubles from 80 mm/d at DVT = 300 kg m^{-1} s^{-1} to 160 mm/d at DVT = 500 kg m^{-1} s^{-1}. Forecasts and predictions of water vapor transport by atmospheric rivers can support flood risk assessment and estimates of future flood frequencies and magnitude in the western United States.

1. Introduction

Atmospheric rivers (ARs) are long (>2,000 km) corridors in the lower troposphere where water vapor is transported poleward at high rates that have been identified as the primary cause of flooding in the western United States (U.S.) (Barth et al., 2017; Dettinger & Ingram, 2013; Dettinger et al., 2011; Florsheim & Dettinger, 2015; Neiman et al., 2011, 2013; Ralph et al., 2006). Geographic variation in the frequency of AR-related flooding across the western U.S. reflects the strong west-to-east gradient in AR-forced precipitation (Barth et al., 2017; Ralph & Dettinger, 2012; Rutz et al., 2014). ARs make landfall on the Pacific Coast more often than floods occur, so there is a great practical need to determine which ARs are most likely to generate floods (Neiman et al., 2008; Ralph et al., 2013) and how changes in water vapor transport by ARs (Lavers et al., 2016; Warner & Mass, 2017) would likely affect flooding. We approach this problem by estimating the probability of high runoff conditioned on water vapor transport in ARs. The results can inform the near-term forecasting of floods, estimation of inflows to reservoirs, and the prediction of changes in flood magnitude and frequency across the western U.S.

2. Data Sets and Analytical Methods

We examine the daily streamflow responses of rivers to atmospheric rivers for water years (1 October to 30 September) 1949 to 2015 over the contiguous U.S. west of the continental divide including the Columbia River basin, the Great Basin, the Colorado River basin, and coastal California, Oregon, and Washington. The analysis is conducted at three spatial scales: individual gaged river basins, grid cells centered at intervals of 2.5° latitude and 2.5° longitude, and the subset of 10 cells that cover the Pacific Coast including the western slope of the Cascade Range and Sierra Nevada (Figure 1). Cells covering the Oregon Coast (−125°W, 45°N) to extreme northern Washington (−122.5°W, 50°N) are excluded due to the small land area of the streamflow gaging network.

2.1. Streamflow and Water Vapor Data

Records of daily mean streamflow spanning at least 10 years from 5,547 gages operated by the U.S. Geological Survey in the western U.S. were compiled for WY 1949–2015 (U.S. Geological Survey, 2016). Streamflow was divided by drainage area at each gage and reported as runoff (mm/d) to standardize river responses to atmospheric rivers. Gages on regulated rivers were included as part of the network for detecting maximum runoff in each 2.5° cell because reservoir releases are unlikely to increase maximum daily runoff at a site during a flood. Regulation may reduce flooding at a site in response to ARs.

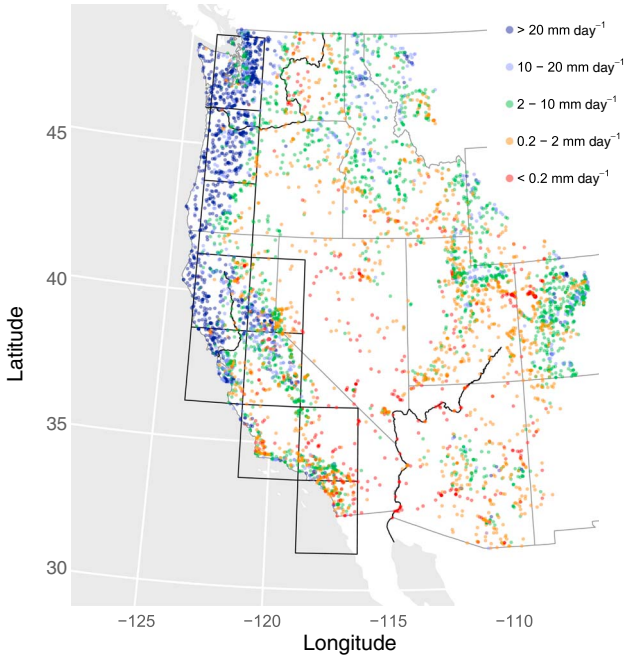

Figure 1. Median annual maximum daily runoff based on available records for water years 1949 to 2015 at 5,477 gages in the western United States. Pacific Coast cells are outlined in black.

We use the National Centers for Environmental Prediction-National Center for Atmospheric Research Reanalysis chronology of vertically integrated water vapor transport (*IVT*) for 2.5° cells reported at 6 h intervals (Kalnay et al., 1996, and updates thereto) with ARs identified by the method of Rutz et al. (2014) as contiguous regions >2,000 km in length that transport water vapor at vertically integrated rates >250 kg m^{-1} s^{-1} for at least 6 h (data accessed at http://www.inscc.utah.edu/~rutz/ar_catalogs/ncep_2.5/timeseries/ on 23 May 2016). Coordinated Universal Times for IVT were converted to Pacific Standard Time (PST). Mean 24 h IVT with lead times of +8, +14, and +20 h was compared to daily streamflow to identify the lead time that best accounted for the generation and routing of runoff from source areas to the reporting gage. Mean 24 h IVT with a 14 h lead best correlates with increased streamflow and is generally representative of the time of concentration of Pacific Coast rivers (Warner et al., 2012), so daily mean vertically integrated water vapor transport (*DVT*) on day *d* refers to the mean of IVT from 10:00 a.m. PST on day $d-1$ to 10:00 a.m. on day *d*.

2.2. Minimum Number of Gages Per Cell

We rely on the U.S. Geological Survey streamflow gaging network to detect the daily maximum runoff response in each 2.5° cell but recognize that the spatial coverage of the network may not be adequate on some days in some cells, which will lead to underestimation of the maximum runoff on a given day. We impose a minimum number of gages as a condition for including a 2.5° cell on a given day based on the likelihood of not detecting high runoff as a function of the number of gages in a cell. Days when a gage met one of four runoff-based criteria were designated as "flood days": (1) daily runoff, *Q*, greater than 50 mm/d and an increase in runoff from the previous day; (2) an increase from the prior day in daily runoff, ΔQ, greater than 30 mm/d; (3) cumulative 3 day runoff, *Q3d*, greater than 150 mm and an increase in runoff from the prior day; or (4) cumulative increase in 3 day runoff from the prior day, $\Delta Q3d$, greater than 90 mm. Cumulative 3 day runoff was assigned to the first day of each 3 day period for comparison with DVT. Overlapping 3 day periods meeting criteria 3 or 4 were filtered to retain only the period with the greatest 3 day runoff or increase in runoff, respectively. While these criteria are used to establish a minimum number of gages as a condition for the analysis and to describe broad patterns of flooding, they are not used to calculate conditional probabilities or runoff responses.

When there are only two gages in a cell, the probability is 18% that both gages met flood criteria conditioned on days when one gage met flood criteria. The conditional probability of two gages recording a flood when one gage records a flood increases rapidly with the number of gages to 52% when there are 5 gages and then gradually to 65% when there are at least 150 gages. We selected 15 gages per cell as a minimum threshold for including observations from a cell on a given day in the analysis.

2.3. Likelihood of Flooding and Limits on Runoff in Relation to Water Vapor Transport

Conditional probabilities that the maximum ΔQ was greater than a threshold, ΔQ^*, when DVT was greater than a threshold, DVT*, were estimated using observations from Pacific Coast cells on days with at least 15 active gages in a cell based on Bayes theorem (Hoel, 1971):

$$P(\Delta Q > \Delta Q^* | \mathrm{DVT} > \mathrm{DVT}^*) = \frac{P(\mathrm{DVT} > \mathrm{DVT}^* | \Delta Q > \Delta Q^*)\, P(\Delta Q > \Delta Q^*)}{P(\mathrm{DVT} > \mathrm{DVT}^*)}. \quad (1)$$

Likewise, the probability that DVT > DVT* when maximum $\Delta Q > \Delta Q^*$ was calculated is as follows:

$$P(\mathrm{DVT} > \mathrm{DVT}^* | \Delta Q > \Delta Q^*) = \frac{P(\Delta Q > \Delta Q^* | \mathrm{DVT} > \mathrm{DVT}^*)\, P(\mathrm{DVT} > \mathrm{DVT}^*)}{P(\Delta Q > \Delta Q^*)}. \quad (2)$$

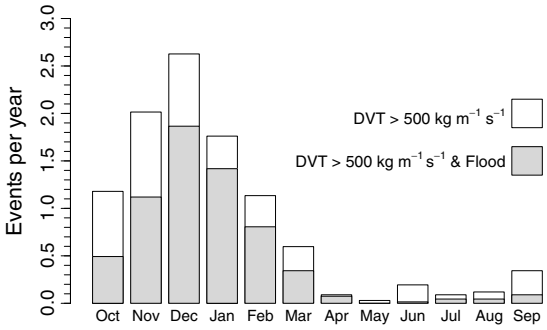

Figure 2. Mean annual number of events (cell days) when daily mean vertically integrated water vapor transport, DVT > 500 kg m^{-1} s^{-1} for 2.5° cells on the Pacific Coast by month (white bar plus gray bar) and mean annual number of events when DVT > 500 kg m^{-1} s^{-1} and a flood in the same cell (gray bar). Each cell where DVT > 500 kg m^{-1} s^{-1} on a given day is counted as an event, so multiple events may occur on the same day. Cell days with fewer than 15 active streamflow gages are not included.

2.4. Maximum Runoff as a Function of Water Vapor Transport

Observation of the maximum increase in runoff for a given rate of water vapor transport can help bracket potential runoff response given incipient AR conditions or forecasts. We relate maximum ΔQ to DVT for each 2.5° cell on days when there was an AR and at least 15 active gages. We apply quantile regression (Koenker et al., 2016) to estimate a linear relation between the 99% quantile of maximum ΔQ and DVT for 2.5° cells on the Pacific Coast (Figure 1).

3. Results

There were 6,351 events (cell days) when runoff in a cell met flood criteria during WY 1949–2015, and 5,417 events (85%) co-occurred with an AR. Multiday ARs were particularly effective at generating floods: 4,373 of 6,351 (76%) events occurred on the second day of an AR. Nearly all events where ΔQ was greater than 100 mm/d (240 of 249 cell days) occurred in response to an AR over the cell. All flood days at 1,187 gages were attributable to ARs.

While most flooding was associated with ARs, many ARs including some that were relatively intense (DVT > 500 kg m^{-1} s^{-1}) did not produce floods. The fraction ARs with DVT > 500 kg m^{-1} s^{-1} that produced floods in Pacific Coast cells increased from 26% in September to 81% in January (Figure 2) potentially indicating diminishing storage capacity of soils and reservoirs from late summer into the winter or the seasonally variable dynamics of ARs (Neiman et al., 2008; Ralph et al., 2013). The fraction of ARs that produce runoff meeting the flood criteria also varies spatially, decreasing from over 30% in the northern Sierra Nevada (40°N, 120°W) and Olympics and western Cascades (47.5°N, 122.5°W) to less than 10% in the interior reflecting lower DVT and less orographic forcing of precipitation.

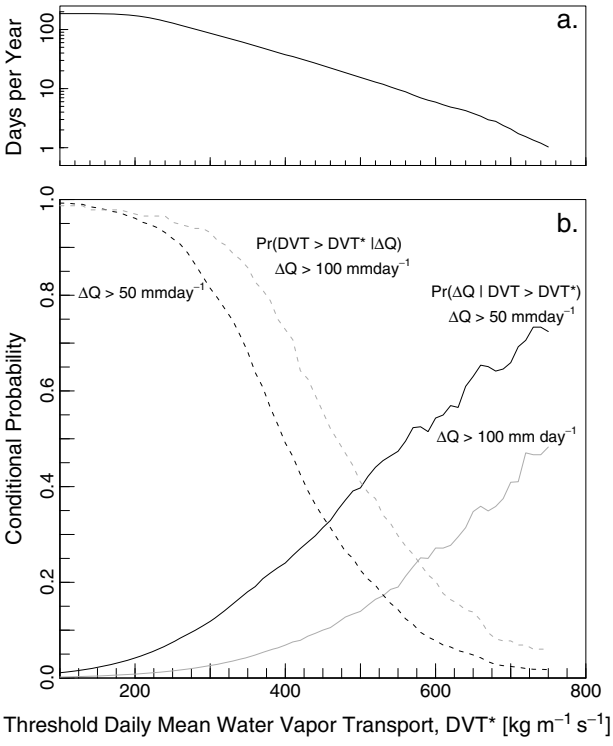

Figure 3. (a) Mean annual frequency that maximum daily mean integrated water vapor transport, DVT, in a 2.5° cell on the Pacific Coast exceeds a threshold, DVT*. (b) Conditional probabilities that the maximum daily change in streamflow, ΔQ > 50 mm d^{-1} when DVT > DVT*(black solid curve), ΔQ > 100 mm d^{-1} (black solid curve) when DVT > DVT*, DVT > DVT* when ΔQ > 50 mm d^{-1} (black dashed curve), and DVT > DVT* when ΔQ > 100 mm/d when DVT > DVT* (gray dashed curve).

3.1. Probability of Floods in Relation to Water Vapor Transport by Atmospheric Rivers

The probability of floods on the Pacific Coast is generally related to both the frequency and intensity of ARs. The mean annual number of ARs is 186 days per year and decreases to ~15 days per year for ARs when DVT > 500 kg m^{-1} s^{-1} (Figure 3a). Conversely, the conditional probability that ΔQ will exceed a given value increases steadily with DVT for a 2.5° cell. For example, the probability that ΔQ > 50 mm/d increases from 12% when DVT > 300 kg m^{-1} s^{-1} to 52% when DVT > 600 kg m^{-1} s^{-1} (Figure 3b). A similar pattern holds for larger increases in runoff, but the probabilities are lower (e.g., $P(\Delta Q > 100$ mm d^{-1} | DVT > 600 kg m^{-1} s$^{-1}) = 27%$).

The probability that DVT exceeds a threshold when runoff increases above a specified level (Figure 3b, dashed curves) indicates the relative contribution to flooding of ARs with DVT above and below the threshold. When ΔQ > 50 mm/d in a 2.5° cell, the probability that DVT > 300 kg m^{-1} s^{-1} is greater than 80% and the probability that DVT > 400 kg m^{-1} s^{-1} is 50%. Thus, ARs with DVT < 300 kg m^{-1} s^{-1} generally do not produce ΔQ > 50 mm/d, but many of the occurrences when ΔQ > 50 mm/d are a result of DVT between 300 and 400 kg m^{-1} s^{-1}. Intense but infrequent ARs are almost certain to produce flooding, but many floods are generated by ARs that are less intense but more common.

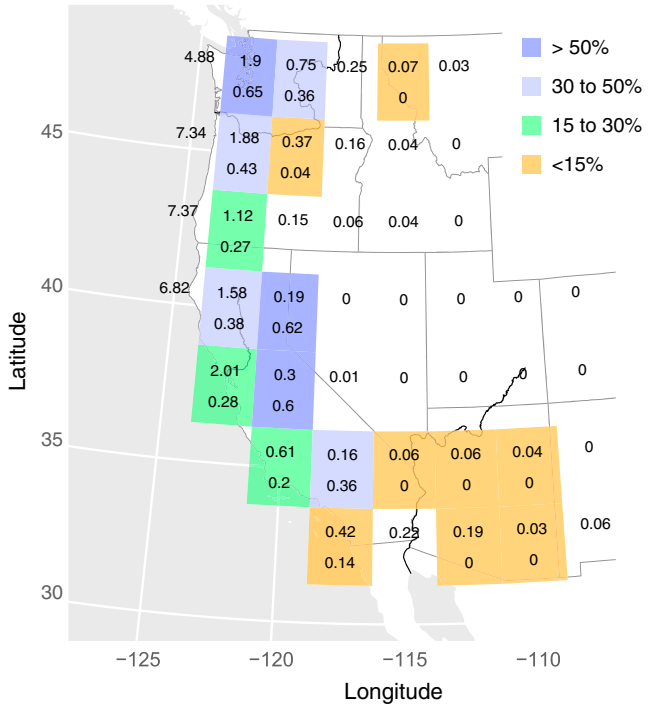

Figure 4. Mean annual frequency (days per year) that daily mean water vapor transport, DVT $>$ 500 kg m^{-1} s^{-1} (upper number) and probability of observing a daily increase in runoff, $\Delta Q > 50$ mm/d in each 2.5° cell (lower number and shading). Cells with less than 15 active gages during all ARs are not shaded but are labeled with annual frequency that DVT $>$ 500 kg m^{-1} s^{-1}.

Runoff responses to water vapor transport by ARs vary within the region. For example, $P(\Delta Q > 50$ mm/d$|$DVT $>$ 500 kg m^{-1} s$^{-1})$ ranges from more than 50% in the western North Cascades and northern and central Sierra Nevada to less than 10% in some of the surrounding cells (Figure 4). The spatial variation in this conditional probability does not depend on AR frequency since "unresponsive" cells represent places spanning the range of AR frequencies. Instead, it appears to represent the combined effects of topographic barriers with the prevailing AR trajectories that force precipitation from ARs.

3.2. Maximum Runoff Response of Pacific Coast Rivers to Water Vapor Transport

Maximum daily increase in runoff observed in a 2.5° cell on the Pacific Coast generally is limited by DVT (Figure 5) and, therefore, can be expected to reflect spatial patterns in DVT, which generally decreases inland (Figure 5a). Annual maximum ΔQ generally decreases from northwest to southeast (Figure 5b). The 99% quantile of ΔQ, $\Delta Q_{0.99}$, can be estimated as an increasing, linear function of DVT:

$$\Delta Q_{0.99} = 0.4\,(\mathrm{DVT} - 100), \tag{3}$$

where the probability that the daily increase in runoff will exceed $\Delta Q_{0.99}$ for any river in a 2.5° cell is 1% given DVT for that cell. When DVT ~ 500 kg m^{-1} s^{-1} in a 2.5° cell, for example, ΔQ has ~ 1% probability of exceeding 160 mm for a river in that cell. The estimate of $\Delta Q_{0.99}$ does not account for geographic variation in AR characteristics or in runoff across the Pacific Coast. This estimate likely is upward biased under dry antecedent conditions of fall and for rivers draining lowland areas and leeward aspects of mountain ranges on the Pacific Coast, with downward biases at higher elevations on the windward aspects of mountain ranges.

4. Discussion of Conditional Flood Responses to Atmospheric Rivers in a Changing Climate

High runoff in the western U.S. from WY 1949 to 2015 occurred primarily during ARs and was restricted largely to coastal ranges and the western Sierra Nevada and Cascade Ranges. This pattern reflects the spatial distribution of frequency of ARs and the increasing intensity of precipitation over high-elevation terrain (Dettinger, 2011; McCabe et al., 2007; Neiman et al., 2008; Ralph & Dettinger, 2012; Rutz et al., 2014). While lowland streams on the Pacific Coast have lower rates of maximum runoff (e.g., Puget Trough, Willamette, and Sacramento River valley), annual maximum streamflow (peaks and mean daily) in these streams is still largely a response to ARs (Barth et al., 2017; Figure S1 in the supporting information).

Climate warming and moistening of the atmosphere in response to increased greenhouse gas concentrations are expected to increase the frequency of ARs and their transport of water vapor (Dettinger, 2011; Lavers et al., 2013). Warner et al. (2015) predict that DVT exceeding ~ 500 to 600 kg m^{-1} s^{-1} along the Pacific Coast will be 3 times more frequent by the end of the 21st century. Changes in flooding can be inferred from projections of enhanced water vapor transport (Lavers et al., 2016; Salathé et al., 2014) by applying the conditional probabilities (Figure 4) and maximum runoff responses (Figure 5) for the Pacific Coast. Such estimates would only be approximate. Actual changes in flooding will depend on the seasonal distribution of changes in water vapor transport (Warner & Mass, 2017) that influence relations between water vapor transport and precipitation (Hagos et al., 2016; Neiman et al., 2008) and between precipitation and runoff (Ralph et al., 2013) and future AR trajectories (Gao et al., 2015; Payne & Magnusdottir, 2015; Radić et al., 2015; Warner et al., 2015). Nevertheless, increased transport water vapor by ARs would likely produce additional flooding runoff along their path. Qualitatively, the projected increases in IVT and AR intensities and

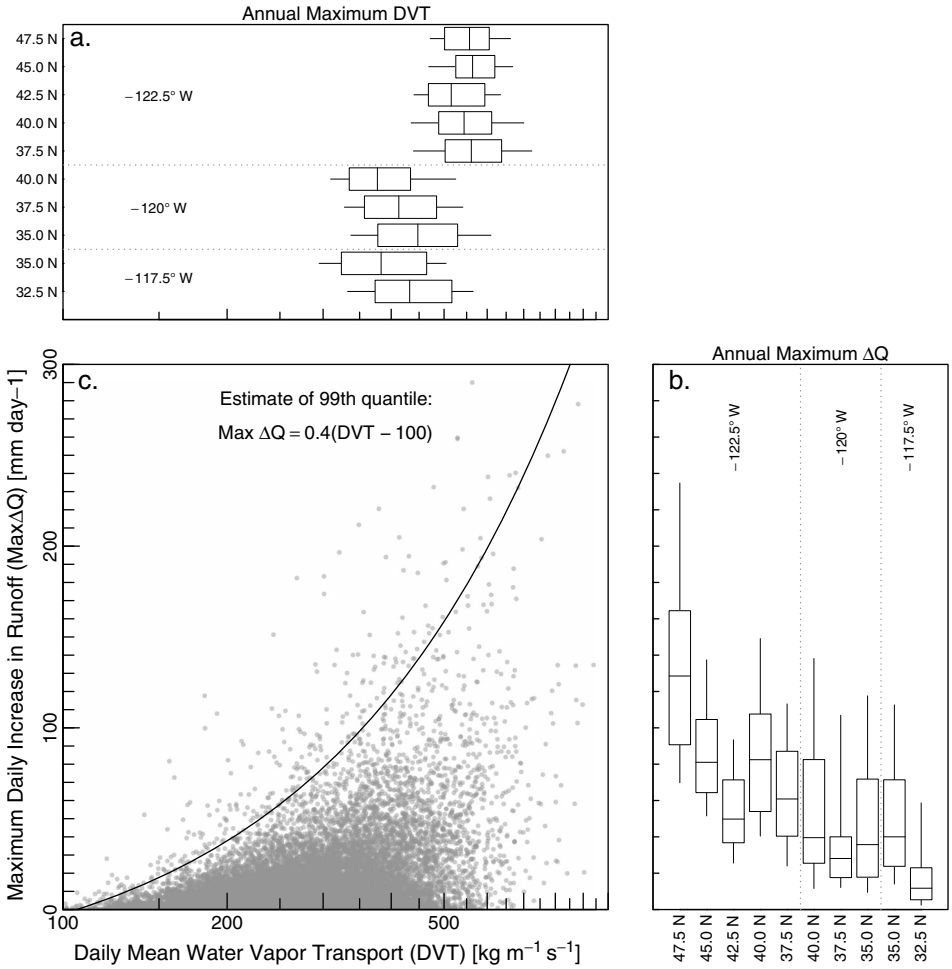

Figure 5. Distributions for each 2.5° cells on the Pacific Coast of (a) annual maximum daily mean water vapor transport, DVT, and (b) annual maximum daily increase in runoff, ΔQ, and (c) maximum ΔQ in each cell as a function of DVT (log scale) on days with ARs. Box and whiskers in Figures 5a and 5b indicate the 10th, 25th, 50th, 75th, and 90th percentiles. The line in Figure 5c represents the 99th quantile of maximum ΔQ and appears curved because of the log scale. Six outliers when maximum ΔQ was greater than 300 mm/d are not shown in Figure 5c.

frequencies as the world warms are consistent with increased frequency and magnitude of future flooding in the western U.S. (Das et al., 2013; Dettinger, 2011; Lavers et al., 2015).

Less intense ARs also represent flood hazards if the ARs make landfall when antecedent soil moisture is high and, in particular, if they occur on consecutive days effectively extending AR duration over a given location (Lamjiri et al., 2017; Ralph et al., 2013; Warner et al., 2012). The cumulative effect of long duration ARs is evident: 76% of AR-associated flooding occurred when an AR persisted for more than a day, but these persistent ARs comprise only 49% of ARs. Even without increased peak rates of water vapor transport, increased frequency and persistence of ARs during wet seasons would increase flooding (Ivancic & Shaw, 2015; Lamjiri et al., 2017; Lavers et al., 2013; Neiman et al., 2013; Vahedifard et al., 2017).

Expectations about precipitation and runoff responses to water vapor transport at a particular location do not have to be bound to a single realization of either observed or simulated ARs at that location (Kunkel et al., 2013; Salathé et al., 2014) but should be tempered by the systematic spatial variation in both AR trajectories and orographic forcing (Figure 4), which influence the amount of runoff generated by landfalling ARs of a given magnitude (Bracken et al., 2015; Dettinger et al., 2004; Hagos et al., 2016; Neiman et al., 2011, 2013; Ryoo et al., 2015). Uncertainties in the future trajectories of ARs, changes in their seasonal timing and water vapor transport, and landscape conditions prevent robust predictions of site-specific changes in flood frequency (Mundhenk et al., 2016; Ralph et al., 2013; Salathé et al., 2014) at this time.

While the flooding impact from changes in moderate ARs (e.g., DVT < 300 kg m^{-1} s^{-1}) would likely depend on seasonal timing and may be limited to river basins with a high propensity for orographic forcing, the increased frequency of larger ARs would very likely increase the frequency of floods particularly on the Pacific Coast. Flooding in the interior West depends on the extent to which ARs will penetrate further inland (Rutz et al., 2015) and, as a result, will be sensitive to future trajectories of ARs and their water vapor transport. Robust quantitative estimation of future flood frequencies for the western U.S. remains a challenge that will require improved prediction of water vapor transport rates, duration, and locations along with its vertical distribution and the vertical distribution of air temperature (Neiman et al., 2013; Payne & Magnusdottir, 2015; Ulbrich et al., 2008; Warner et al., 2015).

5. Summary

ARs generated most of the observed high daily runoff in the western U.S. during water years 1949–2015 particularly along the Pacific Coast. The probability of such floods increases with both the intensity and duration of water vapor transport by ARs. When DVT by an AR exceeds 300 kg m^{-1} s^{-1}, there is a 12% probability that runoff will exceed 500 mm/d in a 2.5° cell under the AR, which increases to 52% when DVT exceeds 600 km m^{-1} s^{-1}. High runoff in response to ARs is more likely during winter months and in locations where land surface topography and AR trajectories force the orographic lift of air laded with moisture. ARs that do not generate floods generally are less intense, shorter duration, have less orographic forcing of precipitation, or occur under dry antecedent conditions. Changes in frequency and magnitude of flooding in the region will depend on the rate and vertical distribution of water vapor transport by ARs in the future and also their seasonal timing and duration over particular locations.

Acknowledgments
Daily streamflow and water vapor transport data are publicly available at https://waterdata.usgs.gov/nwis/dv/?referred_module=sw and http://www.inscc.utah.edu/~rutz/ar_catalogs/ncep_2.5/timeseries/.

References

Barth, N. A., Villarini, G., Nayak, M. A., & White, K. (2017). Mixed populations and annual flood frequency estimates in the western United States: The role of atmospheric rivers. *Water Resources Research*, *53*, 257–269. https://doi.org/10.1002/2016WR019064

Bracken, C., Rajagopalan, B., Alexander, M., & Gangopadhyay, S. (2015). Spatial variability of seasonal extreme precipitation in the western United States. *Journal of Geophysical Research: Atmospheres*, *120*, 4522–4533. https://doi.org/10.1002/2015JD023205

Das, T., Maurer, E. P., Pierce, D. W., Dettinger, M. D., & Cayan, D. R. (2013). Increases in flood magnitudes in California under warming climates. *Journal of Hydrology*, *501*, 101–110. https://doi.org/10.1016/j.jhydrol.2013.07.042

Dettinger, M. D. (2011). Climate change, atmospheric rivers and floods in California—A multimodel analysis of storm frequency and magnitude changes. *Journal of the American Water Resources Association*, *47*(3), 514–523. https://doi.org/10.1111/j.1752-1688.2011.00546.x

Dettinger, M., & Ingram, L. (2013). The coming megafloods. *Scientific American*, *308*(1), 64–71.

Dettinger, M. D., Ralph, F. M., Das, T., Neiman, P. J., & Cayan, D. R. (2011). Atmospheric rivers, floods, and the water resources of California. *Water*, *3*(4), 445–478. https://doi.org/10.3390/w3020445

Dettinger, M. D., Redmond, K. T., & Cayan, D. R. (2004). Winter orographic-precipitation ratios in the Sierra Nevada—Large-scale atmospheric circulations and hydrologic consequences. *Journal of Hydrometeorology*, *5*(6), 1102–1116. https://doi.org/10.1175/JHM-390.1

Florsheim, J., & Dettinger, M. (2015). Promoting atmospheric-river and snowmelt fueled biogeomorphic processes by restoring river-floodplain connectivity in California. In P. Hudson & H. Middelkoop (Eds.), *Geomorphic approaches to integrated floodplain management of lowland fluvial systems in North America and Europe* (pp. 119–141). New York: Springer. https://doi.org/10.1007/978-1-4939-2380-9_6

Gao, Y., Lu, J., Leung, L. Y. R., Yang, Q., Hagos, S. M., & Qian, Y. (2015). Dynamical and thermodynamical modulations of future changes in landfalling atmospheric rivers over North America. *Geophysical Research Letters*, *42*, 7179–7186. https://doi.org/10.1002/2015GL065435

Hagos, S. M., Leung, L. Y. R., Yoon, J.-H., Lu, J., & Gao, Y. (2016). A projection of changes in landfalling atmospheric river frequency and extreme precipitation over western North America from the large ensemble CESM simulations. *Geophysical Research Letters*, *43*, 1357–1363. https://doi.org/10.1002/2015GL067392

Hoel, P. G. (1971). *Introduction to mathematical statistics* (3rd ed., pp. 409). New York: John Wiley.

Ivancic, T. J., & Shaw, S. B. (2015). Examining why trends in very heavy precipitation should not be mistaken for trends in very high river discharge. *Climatic Change*, *133*(4), 681–693. https://doi.org/10.1007/s10584-015-1476-1

Kalnay, E., Kanamitsu, M., Kistler, R., Collins, W., Deaven, D., Gandin, L., … Joseph, D. (1996). The NCEP/NCAR 40-year reanalysis project. *Bulletin of the American Meteorological Society*, *77*(3), 437–471. https://doi.org/10.1175/1520-0477(1996)077%3C0437:TNYRP%3E2.0.CO;2

Koenker, R., Portnoye, S., Ng, P. T., Zeileis, A., Grosjean, P., & Ripley, B. R. (2016). Quantile regression, version 5.29. Retrieved from http://www.r-project.org

Kunkel, K. E., Karl, T. R., Easterling, D. R., Redmond, K., Young, J., Yin, X., & Hennon, P. (2013). Probable maximum precipitation and climate change. *Geophysical Research Letters*, *40*, 1402–1408. https://doi.org/10.1002/grl.50334

Lamjiri, M. A., Dettinger, M. D., Ralph, F. M., & Guan, B. (2017). Hourly storm characteristics along the U.S. West Coast: Role of atmospheric rivers in extreme precipitation. *Geophysical Research Letters*, *44*, 7020–7028. https://doi.org/10.1002/2017GL074193

Lavers, D. A., Allan, R. P., Villarini, G., Lloyd-Hughes, B., Brayshaw, D. J., & Wade, A. J. (2013). Future changes in atmospheric rivers and their implications for winter flooding in Britain. *Environmental Research Letters*, *8*(3), 034010. https://doi.org/10.1088/1748-9326/8/3/034010

Lavers, D. A., Ralph, F. M., Waliser, D. E., Gershunov, A., & Dettinger, M. D. (2015). Climate change intensification of horizontal water vapor transport in CMIP5. *Geophysical Research Letters*, *42*, 5617–5625. https://doi.org/10.1002/2015GL064672

Lavers, D. E., Waliser, D. A., Ralph, F. M., & Dettinger, M. D. (2016). Predictability of horizontal water vapor transport relative to precipitation: Enhancing situational awareness for forecasting western U.S. extreme precipitation and flooding. *Geophysical Research Letters*, *43*, 2275–2282. https://doi.org/10.1002/2016GL067765

McCabe, G. J., Hay, L. E., & Clark, M. P. (2007). Rain-on-snow events in the Western United States. *Bulletin of the American Meteorological Society*, *88*(3), 319–328. https://doi.org/10.1175/BAMS-88-3-319

Mundhenk, B. D., Barnes, E. A., & Maloney, E. D. (2016). All-season climatology and variability of atmospheric river frequencies over the North Pacific. *Journal of Climate*, *29*(13), 4885–4903. https://doi.org/10.1175/JCLI-D-15-0655.1

Neiman, P. J., Ralph, F. M., Moore, B. J., Hughes, M., Mahoney, K. M., Cordeira, J. M., & Dettinger, M. D. (2013). The landfall and inland penetration of a flood-producing atmospheric river in Arizona. Part I: Observed synoptic-scale, orographic, and hydrometeorological characteristics. *Journal of Hydrometeorology*, *14*(2), 460–484. https://doi.org/10.1175/JHM-D-12-0101.1

Neiman, P. J., Ralph, F. M., Wick, G. A., Lundquist, J. D., & Dettinger, M. D. (2008). Meteorological characteristics and overland precipitation impacts of atmospheric rivers affecting the West Coast of North America based on eight years of SSM/I satellite observations. *Journal of Hydrometeorology*, *9*(1), 22–47.

Neiman, P. J., Schick, L. J., Ralph, F. M., Hughes, M., & Wick, G. A. (2011). Flooding in western Washington: The connection to atmospheric rivers. *Journal of Hydrometeorology*, *12*(6), 1337–1358. https://doi.org/10.1175/2011JHM1358.1

Payne, A. E., & Magnusdottir, G. (2015). An evaluation of atmospheric rivers over the North Pacific in CMIP5 and their response to warming under RCP 8.5. *Journal of Geophysical Research: Atmospheres*, *120*, 11,173–11,190. https://doi.org/10.1002/2015JD023586

Radić, V., Cannon, A. J., Menounos, B., & Gi, N. (2015). Future changes in autumn atmospheric river events in British Columbia, Canada, as projected by CMIP5 global climate models. *Journal of Geophysical Research: Atmospheres*, *120*, 9279–9302. https://doi.org/10.1002/2015JD023279

Ralph, F. M., Coleman, T., Neiman, P. J., Zamora, R. J., & Dettinger, M. D. (2013). Observed impacts of duration and seasonality of atmospheric-river landfalls on soil moisture and runoff in coastal northern California. *Journal of Hydrometeorology*, *14*(2), 443–459. https://doi.org/10.1175/JHM-D-12-076.1

Ralph, F. M., & Dettinger, M. (2012). Historical and national perspectives on extreme Pacific Coast precipitation associated with atmospheric rivers during December 2010. *Bulletin of the American Meteorological Society*, *93*(6), 783–790. https://doi.org/10.1175/BAMS-D-11-00188.1

Ralph, F. M., Neiman, P. J., Wick, G., Gutman, S., Dettinger, M., Cayan, D., & White, A. B. (2006). Flooding on California's Russian River: Role of atmospheric rivers. *Geophysical Research Letters*, *33*, L13801. https://doi.org/10.1029/2006GL026689

Rutz, J. J., Steenburgh, W. J., & Ralph, F. M. (2014). Climatological characteristics of atmospheric rivers and their inland penetration over the western United States. *Monthly Weather Review*, *142*(2), 905–921. https://doi.org/10.1175/MWR-D-13-00168.1

Rutz, J. J., Steenburgh, W. J., & Ralph, F. M. (2015). The inland penetration of atmospheric rivers over western North America: A Lagrangian analysis. *Monthly Weather Review*, *143*(5), 1924–1944. https://doi.org/10.1175/MWR-D-14-00288.1

Ryoo, J. M., Waliser, D. E., Waugh, D. W., Wong, S., Fetzer, E. J., & Fung, I. (2015). Classification of atmospheric river events on the US West Coast using a trajectory model. *Journal of Geophysical Research: Atmospheres*, *120*, 3007–3028. https://doi.org/10.1002/2014JD022023

Salathé, E. P., Hamlet, A. F., Mass, C. F., Lee, S. Y., Stumbaugh, M., & Steed, R. (2014). Estimates of twenty-first-century flood risk in the Pacific Northwest based on regional climate model simulations. *Journal of Hydrometeorology*, *15*(5), 1881–1899. https://doi.org/10.1175/JHM-D-13-0137.1

U.S. Geological Survey (2016). National Water Information System. Retrieved from https://waterdata.usgs.gov/nwis/dv/?referred_module=sw, accessed 2 November 2016.

Ulbrich, U., Pinto, J. G., Kupfer, H., Leckebusch, G. C., Spangehl, T., & Reyers, M. (2008). Changing Northern Hemisphere storm tracks in an ensemble of IPCC climate change simulations. *Journal of Climate*, *21*(8), 1669–1679. https://doi.org/10.1175/2007JCLI1992.1

Vahedifard, F., Agah Kouchak, A., Rangno, E., Shahrokhabadi, S., & Mallakpour, I. (2017). Lessons from the Oroville dam. *Science*, *355*(6330), 1139–1140. https://doi.org/10.1126/science.aan0171

Warner, M. D., & Mass, C. F. (2017). Changes in the climatology, structure, and seasonality of northeast Pacific atmospheric rivers in CMIP5 climate simulations. *Journal of Hydrometeorology*, *18*(8), 2131–2141. https://doi.org/10.1175/JHM-D-16-0200.1

Warner, M. D., Mass, C. F., & Salathé, E. P. (2012). Wintertime extreme precipitation events along the Pacific Northwest coast: Climatology and synoptic evolution. *Monthly Weather Review*, *140*(7), 2021–2043. https://doi.org/10.1175/MWR-D-11-00197.1

Warner, M. D., Mass, C. F., & Salathé, E. P. (2015). Changes in winter atmospheric rivers along the North American west coast in CMIP5 climate models. *Journal of Hydrometeorology*, *16*(1), 118–128. https://doi.org/10.1175/JHM-D-14-0080.1